HEAT PROPAGATION DYNAMICS IN THIN CLASSICAL SEMICONDUCTORS

Katalin Gambár – Ferenc Márkus

1. ABSTRACT

On nanoscale the sample size has an explicit contribution to the behaviour of the heat transport. In this paper we point out the necessity to take into account not only the size parameter of the material bulk but its boundary since the wall effects play important role in the reflections and scatterings of the phonons. The present mathematical calculations are based on the fluctuation dissipation theory. We calculate the spectra and the related time correlation functions by which the fundamental change of the dynamics of signal propagations can be examined in thin (60 nm and 100 nm) semiconductor (especially silicon) layers.

2. INTRODUCTION

The experimental data [1,3] and the computational calculations [4,5] indicate that on nanoscale the description of transport requires new mathematical model. By decreasing the sample size the ballistic propagation appears beside the diffusive transport. It seems obvious that we need to take into account both the size and the boundary effects [6-11]. In the present paper to involve the thermal inertial effects we apply a dual-phase-lag constitutive equation suggested by D.Y. Tzou [12-14] and Anderson-Tamma [15]. Their central equation is based on statistical considerations of phonons described by the Boltzmann transport equation. In **physics,** a phonon is a **collective excitation** in a periodic, elastic arrangement of **atoms** or **molecules** in condensed matter, such as **solids** and some **liquids.** We accepted this formulation and constructed the relevant physical equations taking into account size and boundary conditions. We applied the fluctuation dissipation theory to study propagation modes by calculating the wave number - frequency spectra and the time correlation functions.

3. SIZE EFFECTS AND BOUNDARY CONDITIONS

In order to study the possible thermal propagations in nanolayers, we need to formulate the physical equations. The conservation of the internal energy

$$\varrho c_v \frac{\partial T}{\partial t} + \frac{\partial q}{\partial x} = 0, \tag{1}$$

where T is the temperature, q is the x component of the heat flux, ϱ is the mass density and c_v is the specific heat at constant volume. The generalized constitutive equation can be deduced from the one dimensional Anderson-Tamma model [15]

$$q + \tau \frac{\partial q}{\partial t} = -K\left[\frac{\partial T}{\partial x} + \tau \frac{K_F}{K}\frac{\partial}{\partial t}\left(\frac{\partial T}{\partial x}\right)\right] \tag{2}$$

that involves the inertial effects. Here, T is the temperature, q is the x component of the heat flux, τ is the relaxation time, the heat conductivity K relates to the bulk, the coefficient K_F should be considered as an additional conductivity factor. The experimental results show [16,17] and Alvarez's and Jou's [18] studies – how the mean free path of the phonons influences the transport – mathematically proved that the conductivity parameters coefficient K and the coefficient K_F depend on the width of the film, i.e.

$$K(\{Kn\}) = \frac{K}{2\pi^2\{Kn\}^2}\left[\sqrt{1 + 4\pi^2\{Kn\}^2} - 1\right], \tag{3}$$

$$K_F(\{Kn\}) = \frac{K_F}{2\pi^2\{Kn\}^2}\left[\sqrt{1 + 4\pi^2\{Kn\}^2} - 1\right]. \tag{4}$$

Here, $\{Kn\}$ is the Knudsen-number which is the ratio of the mean free path l of the phonons and the width L of the layer

$$\{Kn\} = \frac{l}{L}. \tag{5}$$

The bulk conductivity can be obtained by taking the limit $L \to \infty$. We mention that in spite of that the conductivity parameters involve the size of the bulk; the boundary contribution is not taken into account in all aspects because the wall effects have not appeared explicitly. Detailed studies [4,19] of phonon reflections and scatterings on the boundaries lead to the equation

$$\tau_b \frac{\partial T}{\partial t} + T = T_h - qR, \tag{6}$$

where the coefficient τ_b pertains to the temperature relaxation on the wall. Now, the measurable fluctuating wall temperature T_h has a feedback from the layer. The term $-qR$ pertains to the heat conductivity resistance; R is a parameter. This contact thermal resistance has been experimentally justified [20].

4. SPECTRA AND CORRELATION FUNCTIONS

A possible examination technique of the propagation modes is via the time correlation functions. To achieve this aim we calculate the wave number - frequency spectrum $S(k,\omega)$, by its inverse Fourier transform we obtain the time correlation function $C(k,t)$. In the mathematical elaboration it is useful to apply dimensionless variables [21,22] introducing a reference temperature T_0, thus new variables are introduced by the following transformations: instead of the temperature T

$$a_1 = \frac{T}{T_0}, \tag{7}$$

the heat current q

$$a_2 = \left(\frac{\tau}{T_0^2 K \varrho c_v}\right)^{1/2} q \tag{8}$$

and the fluctuating wall temperature T_h

$$a_3 = \frac{T_h}{T_0}. \tag{9}$$

The physical equations can be reformulated by those variables, i.e., the energy balance in Eq. (1) will be

$$\frac{\partial a_1}{\partial t} + \left(\frac{K(\{Kn\})}{\varrho c_v \tau}\right)^{1/2} \frac{\partial a_2}{\partial x} = 0, \tag{10}$$

the constitutive equation in Eq. (2)

$$\frac{1}{\tau} a_2 + \frac{\partial a_2}{\partial t} = -\left(\frac{K(\{Kn\})}{\varrho c_v \tau}\right)^{\frac{1}{2}} \left[\frac{\partial a_1}{\partial x} + \tau \frac{K_F(\{Kn\})}{K(\{Kn\})} \frac{\partial}{\partial t}\left(\frac{\partial a_1}{\partial x}\right)\right], \tag{11}$$

and the boundary effect in Eq. (6)

$$\tau_b T_0 \frac{\partial a_1}{\partial t} + T_0 a_1 = T_0 a_3 - \left(\frac{T_0^2 K(\{Kn\}) \varrho c_v}{\tau}\right)^{1/2} R a_2. \tag{12}$$

To apply the fluctuation-dissipation theorem we transform Eqs. (10) and (11) to Fourier's space

$$\omega \hat{a}_1 + \left(\frac{K(\{Kn\})}{\varrho c_v \tau}\right)^{1/2} k \hat{a}_2 = 0, \tag{13}$$

$$\hat{a}_2 + i\omega\tau \hat{a}_2 = -\left(\frac{K(\{Kn\})\tau}{\varrho c_v}\right)^{\frac{1}{2}} \left[ik\hat{a}_1 - \tau \frac{K_F(\{Kn\})}{K(\{Kn\})} \omega k \hat{a}_1\right] + \hat{f}, \tag{14}$$

where $\hat{a}_1$ and $\hat{a}_2$ denote the Fourier transformed, $\hat{f}$ means Gaussian stochastic fluctuations. From those equations such the wave number - frequency spectrum

$$S(k,\omega) = \frac{K(\{Kn\})k^2}{\left(\frac{K(\{Kn\})}{\varrho c_v} k^2 - \tau\omega^2\right)^2 + \left(1 + \tau \frac{K_F(\{Kn\})}{\varrho c_v} k^2\right)^2 \omega^2} \tag{15}$$

can be calculated in which the finite size appears due to the Knudsen-number however there is no involved boundary effect. To achieve this take we calculate the half-Fourier transform of Eqs. (10) and (12), then the Laplace transform of the obtained equation. Solving the equations, we got the boundary controlled wave number - frequency spectrum, finally

$$S_b(k,\omega) = \left[\left(1 + \sigma\tau_b - \varrho c_v R \frac{\omega}{k}\right)^2 + \left(\tau_b \omega + \frac{\varrho c_v R \sigma}{k}\right)^2\right] \times \frac{K(\{Kn\})k^2}{\left(\frac{K(\{Kn\})}{\varrho c_v} k^2 - \tau\omega^2\right)^2 + \left(1 + \frac{\tau K_F(\{Kn\})}{\varrho c_v} k^2\right)^2 \omega^2} \tag{16}$$

Furthermore, the spectrum involves the property of the dynamic critical phenomena of the system. The factor in the bracket [...] gives an extra contribution for the higher ω frequencies. This is proportional to ω^2 for high frequencies, but the second factor decreases with ω^4, thus $S_b(k, \omega \to \infty) \to 0$. The spectrum $S_b(k,\omega)$ turns into the "boundary-free" situation for thick bulks in that case when $R = 0$ and $\tau_b = 0$ in the factor. For the low values of frequencies this factor has a minimal value decreasing their contribution.

The time correlation function $C(k,t)$ is the inverse Fourier transforms of the spectrum $S(k,\omega)$

$$C(k,t) = \frac{1}{\sqrt{2\pi}} \int_{-\infty}^{\infty} S(k,\omega) e^{i\omega t}\, d\omega. \tag{17}$$

By the study of the correlation functions we can classify the different signal propagation modes. After the presented calculations and discussions, finally, we can conclude that both the size of the system and the boundary effects are taken into account within this calculation as it is suggested by the Refs. [4,19].

5. THE GRAPHICAL ANALYZIS FOR THE SILICON

We show on detailed examples how the propagation dynamics changes as the function of such parameters like the wave number k, the Knudsen-number $\{Kn\}$, the damping factor σ, the resistance parameter R and the relaxation time τ_b. The physical properties of silicon are measured accurately, thus we apply its parameters: mass density $\varrho = 2330$ kg/m^3, the specific heat at constant volume $c_v = 710$ J/kgK and bulk heat conductivity $K = 149$ W/mK. The value of the heat conductivity of retardation K_F is an adjusting parameter; we take $K_F = 10$ W/mK. The mean free path of the phonons in silicon is $l = 200$ nm; the temperature can be arbitrary at this stage, $T_0 = 1$ K. To see the difference in the signal propagation due to the layer thick, it is taken $L_1 = 100$ nm and $L_2 = 60$ nm. The figures below show both the wave number - frequency spectra $S_b(k,\omega)$ and the time correlation functions $C(k,t)$ for different wave numbers for the Knudsen-numbers $\{Kn\}_1 = l/L_1 = 2$ and $\{Kn\}_2 = l/L_2 = 3.33$.

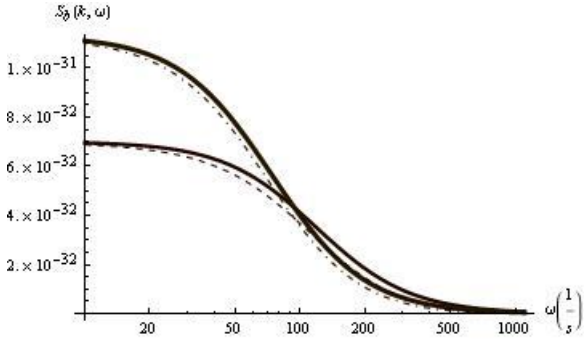

Figure 1.
Spectrum (low frequency)

Due to the wide range of frequency ω it is easier to recognize the change in the spectra if we consider first the low frequency part of the spectra to $\omega\sim1000s^{-1}$ for the two pairs of parameters [$R = 0$ m^{2}K/W; $\tau_b = 0$ s; $\sigma = 1$ s^{-1} and $R = 1\times10^{-6}$ m^{2}K/W; $\tau_b = 5\times10^{-10}$ s; $\sigma = 1$ s^{-1}] at $k = 3000$ m^{-1} can be seen in Fig. 1. The Knudsen-numbers are $\{Kn\}_1 = 2$ and $\{Kn\}_2 = 3.33$; the curves are plotted in one graph at the given parameter set. The curves for the higher Knudsen-number have higher values, these move to the left, i.e., the smaller frequencies have greater contribution to the signal propagation. The changes of the spectra are more explicit on high frequencies. While the spectra tend to zero in the case $R = 0$ m^{2}K/W; $\tau_b = 0$ for big ω values, the situation is strongly different (exactly the reverse) for $R = 1\times10^{-6}$ m^{2}K/W; $\tau_b = 5\times10^{-10}$ s. The curves, in Fig. 2. show well that in the boundary-involved cases the appeared high frequencies have a huge role in the change of signal propagation. The solid tails pertain to the case $R = 0$ m^{2}K/W; the thin curve (left-above) is for $\{Kn\}_1 = 2$, the other one is (left-below) is for $\{Kn\}_2 = 3.33$. The thin-dashed curve is for $\{Kn\}_1 = 2$, the thin-dot-dashed curve is for $\{Kn\}_2 = 3.33$. The appeared wide plateau in the spectrum between the frequencies $\omega\sim10^5 - 10^{11}$ s^{-1} is higher for the higher values of R, i.e., the contribution of the higher frequency modes is greater with the increase of R. Those spectra involve the new physics in the present transport phenomenon, i.e., a different thermal propagation through the film. The property of the signal propagation can be concluded from the time correlation function. The graph in Fig. 3. shows the time correlation functions at $k = 3000$ m^{-1} for the $\{Kn\}_1 = 2$ (thin-solid line) and $\{Kn\}_2 = 3.33$ (thick-solid line).

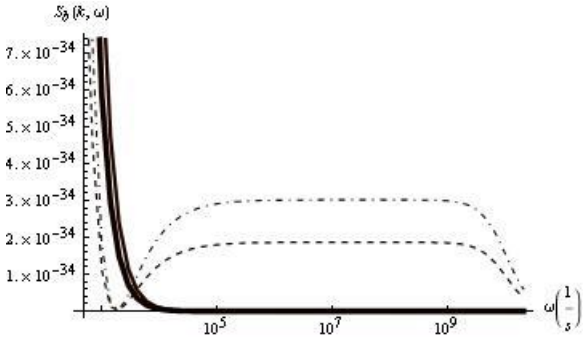

Figure 2.
Spectrum (high frequency)

Those curves show that for both Knudsen-numbers at $k = 3000$ m^{-1} with neglected boundary contribution $R = 0$ m^{2}K/W; $\tau_b = 0$ s the signal propagation is decaying (D). The characteristic time is in the order of 10^{-4} s; and the higher Knudsen-number (thinner film) causes higher correlation values at time $t = 0$ s. However, by the increasing the wave numbers up to very high values the oscillating (O) propagation modes appear as it can be seen in Fig. 4. The change of the behaviour of the signal propagation can

be concluded not only from the change of the shape of the correlation function but from the enormous change of the characteristic time, which is in the order of 10^{-12} s. The correlation time decreases as the wave number increases, thus the appeared short characteristic time $\sim 10^{-12}$ s is not surprising. But we will see soon why the scale jump is important. The thick-solid line belongs to $k = 10^7$ m^{-1}; the thin-dotted and solid line pertains to $k = 1.8 \times 10^7$ m^{-1}. The oscillating behaviour can be recognized obviously in the case of $k = 1.8 \times 10^7$ m^{-1}. The exact transition value between (D) and (O) is at the critical $k = 1.4 \times 10^7$m^{-1} ($R = 0$ m^{2}K/W; $\tau_b = 0$ s).

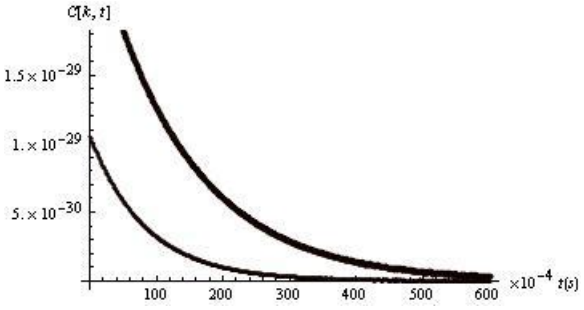

Figure 3.
Correlation without boundary

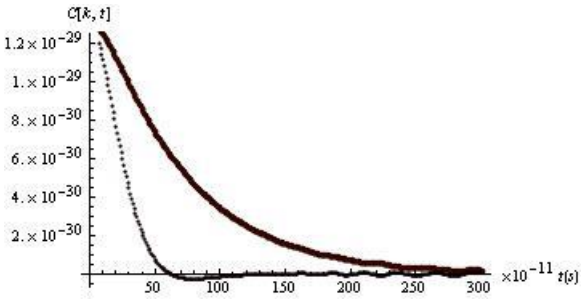

Figure 4.
Correlation (O) (D)

Now, we return to the calculation of the correlation functions for small wave numbers introducing the boundary effects. The correlation functions are calculated at $k = 3000$ m^{-1} taking into account the boundary effects with the parameters $R = 1 \times 10^{-6}$ m^{2}K/W; $\tau_b = 5 \times 10^{-10}$ s for the $\{Kn\}_1 = 2$ (thin-solid line) and $\{Kn\}_2 = 3.33$ (thick-solid line). The effect is obvious from the plot of the curves in Fig. 5; in spite of the small value of R, and τ_b, the correlation functions are changed radically, the time-scale has been converted to 10^{-12} s from 10^{-4} s. The (D) behaviour turned into the (O) due to the direct consequence of the boundary effects.

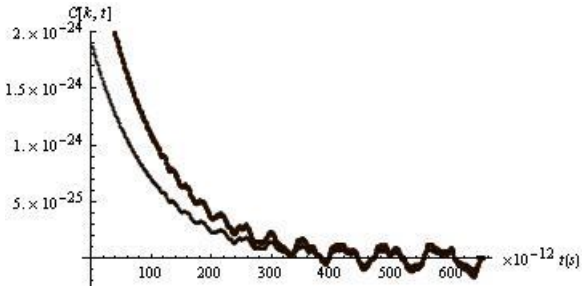

Figure 5.
Correlation with the boundary

6. SUMMARY AND CONCLUSIONS

In this paper we have presented a new mathematical model based on physical considerations by which boundary controlled dynamic phase transition of the thermal signal propagation in thin semiconductor layers can be successfully treated. The further aim is to study the effects of the crystal orientation and defects of the silicon layers, moreover, to widen this description for electric transport, and examine the cross effects.

7. REFERENCES

[1] J. Wang, J.-S. Wang, Appl. Phys. Lett. **88** (2006) 111909.
[2] D.G. Cahill, W.K. Ford, K.E. Goodson, G.D. Mahan, A. Majumdar, H.J. Maris, R. Merlin, S.R. Phillpot, J. Appl. Phys. **93** (2003) 793.
[3] E. Brown, L. Hao, J.C. Gallop, J.C. Macfarlane, Appl. Phys. Lett. **87**, 023107 (2005).
[4] G. Chen, Phys. Rev. Lett. **86** (2001) 2297.
[5] A.S. Henry, G. Chen, J. Comput. Theor. Nanosci. **5** (2008) 1.
[6] G.D. Mahan, F. Claro, Phys. Rev. B **38** (1988) 1963.
[7] F.X. Alvarez, D. Jou, A. Sellitto, J. Appl. Phys. **105** (2009) 014317.
[8] D. Jou, A. Sellitto, F.X. Alvarez, Proc. R. Soc A **467** (2011) 2520.
[9] D.D. Joseph, L. Preziosi, Rev. Mod. Phys. **61** (1989) 41.
[10] G. Lebon, M. Grmela, C. Dubois, C.R. Mech. **339** (2011) 324.
[11] G. Lebon, H. Machrafi, M. Grmela, C. Dubois, Proc. R. Soc. A **467** (2011) 3241.
[12] D.Y. Tzou, Int. J. Heat and Mass Transfer **38** (1995) 3231.
[13] D.Y. Tzou, Macro- to microscale heat transfer: the lagging behaviour, Taylor and Francis, Washington, 1997.
[14] D.Y. Tzou, Z.-Y. Guo, Int. J. Thermal Sci. **49** (2010) 1133.
[15] C.D.R. Anderson, K.K. Tamma, Phys. Rev. Lett. **96** (2006) 184301.

[16] W. Liu, M. Asheghi, Appl. Phys. Lett. **84** (2004) 3819.
[17] Y.S. Ju, K. E. Goodson, Appl. Phys. Lett. **74** (1999) 3005.
[18] F.X. Alvarez, D. Jou, Appl. Phys. Lett. **90** (2007) 083109.
[19] F.X. Alvarez, D. Jou, J. Heat Trans. **132** (2010) 012404.
[20] Z. Chen, W. Jang, W. Bao, C.N. Lau, C. Dames, Appl. Phys. Lett. **95** (2009) 161910.
[21] A.J. McKane, F. Vázquez, Phys. Rev. E **64** (2001) 046116.
[22] F. Márkus, K. Gambár, Int. J. Heat and Mass Transfer **56** (2013) 495.